Etching and optical properties of 1–2 MeV alpha particles irradiated CR-39 radiation detectors

K.C.C. Pires [a],*, M. Assunção [b], M.A. Rana [c,1], S. Guedes [d], R. Künzel [b], N.M. Trindade [e,a]

[a] Departamento de Física Nuclear, Instituto de Física, Universidade de São Paulo, 05508-090, São Paulo, Brazil
[b] Departamento de Física, Universidade Federal de São Paulo, Campus Diadema, 09972-270, São Paulo, Brazil
[c] MERADD, Instrumentation Control and Computer Complex (ICCC), PARAS Building, 18-KM Multan Road, P.O. Chung, Lahore, Pakistan
[d] Instituto de Física Gleb Wataghin, Universidade Estadual de Campinas, 13083-859, São Paulo, Brazil
[e] Department of Physics, Federal Institute of Education, Science and Technology of São Paulo, São Paulo, 01109-010, Brazil

ABSTRACT

A comparison of track etch parameters at low energy alpha particles is presented, using the Lantrak and the Baryotrak CR-39 nuclear track detectors. Experimental data from literature, obtained through exposing CR-39 detectors at low energy alpha particles from a ^{241}Am source and, subsequently, etching them in NaOH, KOH, and NaOH+ethyl alcohol aqueous solutions at 70 °C and 80 °C, have been numerically analyzed here. Radial etch rates of alpha particle etch pits have been determined, compared, and critically discussed for both CR-39 types. Ratios of alpha etch pit diameters and etch pit densities have also been examined as a function of etching time, showing no notable differences in the comparison between these two detectors. This study has been extended from the structural point of view by performing new Ultraviolet–visible (UV–Vis) and Raman spectroscopy measurements on non-irradiated, α-irradiated and α-irradiated/etched Lantrak and Baryotrak detectors. The direct band-gap energies have been determined and no significant differences have been observed in detectors subjected to different conditions. The Raman spectra show that the CH$_2$ functional group has been decreased when comparing the non-irradiated/α-irradiated and α-irradiated/etched detectors, suggesting a degradation of the detectors due to alpha particle irradiation and also due to the different chemical etching treatments applied. The uncertainties have been determined and reported along with the results.

1. Introduction

Nuclear track detectors (NTDs) are commonly applied to radiation detection and environmental monitoring, mineralogy, dosimetry and other applications [1–6]. An energetic charged particle, penetrating in a nuclear track detector, leaves behind it a damaged trail of a nanoscale diameter, commonly called a latent track. An appropriate chemical etching is used to develop, or enlarge, the latent track up to micrometer scaling conical structure, called nuclear track [7]. Alpha particle and fission fragment tracks are the most commonly investigated nuclear tracks [1].

The Columbia Resin No. 39 (CR-39) is a widely used NTD [8–14]. The study of the CR-39 polymer started a few decades ago [15]. Relevant contributions on nuclear track field were given from the first meeting in 1957, which evolved into well-established and regular meetings. Currently the "International Conference on Nuclear Tracks in Solids" has been organized by the International Nuclear Track Society (INTS) and traditionally discussed the nuclear tracks methodology, which contributes to an immense number of applications across a wide

range of scientific and technological fields. Proceedings of these conferences are rich sources of information about nuclear track detectors and their applications, providing overviews on the developments in this field [16]. In particular, in the latest editions of this conference series, there are several works based on studies of chemical etching on alpha particle tracks [17–20]. Specifically in CR-39 detectors, the alpha tracks have been studied using experimental, computational and theoretical tools targeting a number of applications. Here, we briefly highlight the work involving the detection of alpha particles by this type of detector, starting with *Fews and Henshaw* (1982) [21], who present an important investigation of high energy alpha spectroscopy, using CR-39 detectors with resolution of 20 keV for 6 MeV alpha particles. *Sohrabi and Zainali* (1986) have applied the electrochemical etching method for an efficient etching of alpha tracks in CR-39 [22]. *Bing* (1993) has improved a radon measurement methodology using CR-39 through alpha track measurement [23]. *Tavares and Terranova* (1997) have presented a method for the measurement of alpha particle activity at long-lived radioisotopes like ^{190}Pt [24]. *Dörschel et al.* (2003) have reported a 3D

---

* Corresponding author.
  E-mail address: kelly@if.usp.br (K.C.C. Pires).
[1] Present address: Department of Physics, Lahore Garrison University, DHA Phase VI Sec-C, Lahore, Pakistan.

shape computation of etched alpha tracks in CR-39 [25]. *Nikezic and Yu* (2003) have developed a computer code to calculate alpha etched track parameters and profiles [26]. *Rana* (2008) has used the *Nikezic and Yu* computer code [26] to discuss the reliable predictions of alpha tracks in CR-39 detectors [27]. *Azooz et al.* (2012) have investigated the parametrization of alpha track profiles in CR-39 [28]. *Fan et al.* (2017) have presented results on uncertainty of an automatic system for counting alpha tracks in CR-39 detectors [29]. *Chavan et al.* (2021) have presented a new recording method for the quantification of ultratrace alpha radioactivity in medium solution using CR-39 detectors [30]. Still in 2021, *Oliveira et al.* have examined the 1–2 MeV alpha track diameter and density under different etching conditions for two types of CR-39 detector [31].

Moreover, alpha particles are present in neutron monitoring for the boron neutron capture therapy (BNCT) [3], personal neutron dosimetry [32] and secondary neutron monitoring in radiotherapy equipaments [33] consisting of important applications of boron converters/CR-39 detectors. Studies employing CR-39 as detectors in neutron capture radiography are based on the same principles, but includes the boron in the sample to be analyzed [34,35].

In this work, we provide an in-depth and quantitative analysis of published experimental data, which reveals unexplored aspects. To support data analysis, new Ultraviolet–visible (UV–Vis) and Raman spectroscopy measurements have been performed. The spectroscopic analysis adds important information on the mechanisms underlying CR-39 detection efficiency.

The article is organized as follows. In Section 2, we briefly comment on the experimental procedure of CR-39 detectors exposure to alpha particles, chemical etching of exposed detectors, measurement of track parameters and statistical analysis. In Section 3, we show our experimental results, including the discussion about radial etch rate, ratio of alpha etch pit diameters and densities, optical response and results of Raman spectroscopy. Finally, in Section 4 we summarize the main conclusions of our paper.

2. Summary of the experimental data

In this work, the experimental data on the etching of alpha tracks on CR-39 and their uncertainties have been extracted from *Oliveira et al.* [31], in which essential details of the experiments may be found. In what follows, a brief summary of the relevant information on the exposure of detectors, chemical etching, and alpha track measurements is provided. Two types of CR-39 detectors, Lantrak and Baryotrak, have been exposed to low energy alpha particles, using a thin planar alpha source of ^{241}Am (E_α = 5.486 MeV). The detector-source set has been kept fixed at 41.36 mm apart, in air, which resulted in a 1.5 ± 0.5 MeV alpha particle energy on the detector. This energy was determined by an alpha spectrometric method [36]. Because of the large uncertainty, through the rest of the analysis, it is preferred to refer to an energy range (1–2 MeV), rather than pointing to a specific energy value. The step etch experiments were carried out in three different aqueous etching solutions, namely KOH (30% in mass), 6.25 M NaOH and 6.25 M NaOH + 2% ethyl alcohol, and at two different temperatures: 70 and 80 °C. The thickness of the CR-39 detectors used in this work suffered a variation due to chemical treatment. Virgin (not irradiated and not etched) CR-39 detectors are up to 9% thicker than the ones subjected to chemical etching. In this context, the average value of the detectors thickness employed in this work before and after the chemical etching were 0.814 ± 0.003 mm and 0.740 ± 0.019 mm, respectively. The chemical etching has been carried out at regular short intervals of time, thereby permitting the study of the etch pit diameter growth, in addition to the surface etch pit density behavior for both detectors. After each step of etching, etch pits have been observed, at the same positions, employing a Leitz Diaplan optical microscope with magnification of 78.75× [31].

In measurements with NTD detectors, there usually are some sources of uncertainty, such as variation in the latent track lengths for alpha

particles of the same energy and the spread of incident alpha particle energies, variations in the etching solution concentration and temperature from set values, and the limited accuracy of the optical microscope used in measurements of the etched alpha tracks [31]. The mentioned uncertainty sources are reflected in the standard deviations of etch pit diameter and surface density distributions.

Here, we also present new experimental measurements, using the Ultraviolet–visible (UV–Vis) and Raman spectroscopy techniques. The UV–Vis technique has been employed to investigate any possible changes in the CR-39 detectors absorbing spectra, induced by the alpha particles irradiation, and also to know how these detectors are affected by the etching process at different temperatures. An UV–Vis spectrophotometer (Shimadzu, model UV-2600), equipped with an Integrating Sphere Assembly, has been used for the absorption measurements in the 200–800 nm wavelength range, with a 0.1 nm wavelength resolution. The UV–Vis measurements have been performed using a non-irradiated, α-irradiated and α-irradiated/etched Lantrak and Baryotrak CR-39 detectors (the last one from Ref. [31]), employing air as a reference. The irradiation has been performed using the same alpha particle source, setup and geometry described in Ref. [31] for 6.5 hours of exposure. The non-irradiated detectors have been used as a reference. These measurements have been normalized by the maximum absorbance value for each spectrum. Moreover, Raman spectra measurements have been carried out for all detectors using a Raman Renishaw microscope, InVia model, with a multichannel CCD detector and He–Ne (632.8 nm) excitation laser, and a grating system with 1800 l/mm. Data has been registered with the option of automatic cosmic ray removal. Spectra have been collected in the range 600–3200 cm^{-1}. In the Raman spectra, the background signal has been subtracted adopting a fifth-order polynomial function based on the least-squares fitting method. In addition, the Savitzky–Golay smoothing filter has been applied. After that, each spectrum has been normalized to the unity area to minimize the effect of variations on the thickness of the detectors.

3. Results and discussion

3.1. Radial etch rates

According to Ref. [31], the alpha tracks etched in the KOH, NaOH, and NaOH + ethyl alcohol aqueous solutions are the largest, smallest, and intermediate, respectively, in diameter size for both Lantrak and Baryotrak detectors at 70 °C and 80 °C. The same tendency of diameter growth for both detectors, and also at the same temperatures, suggest that the procedures of chemical etching have been precise and reproducible. The effects of the ethyl alcohol addition on the behavior of the track diameters have been investigated for NaOH solutions. In this case, the alpha etch pit diameter ratio (D_r) has been defined and calculated for different regular etching time intervals through

$$D_r = \frac{D_{NA}}{D_N}, \tag{1}$$

where D_{NA} and D_N are the alpha etch pit diameters for etching in NaOH + ethyl alcohol and NaOH aqueous solutions, respectively. The plots of D_r can be seen in Fig. 1.

The first notable feature that arises regards the D_r values, which are consistently higher for Baryotrak, thereby indicating that this type of detector is more sensitive to the addition of ethyl alcohol than does the Lantrak one. Also, the addition of ethyl alcohol to the etching solution makes the etch pit diameters larger in Baryotrak ($D_r > 1$, Fig. 1-(a) and -(c)). Although less evident, the same behavior is observed for Lantrak, etched at 70 °C. An exception is observed exclusively in the case of only long time etching (beyond 600 min) of Lantrak CR-39 at 80 °C, for which $D_r < 1$. The reason for this may have been minute evaporation, or leakage, of ethyl alcohol from the etching solution during the procedure, despite the special care that has been taken to deal with the etching beaker, which must be leakage tight.
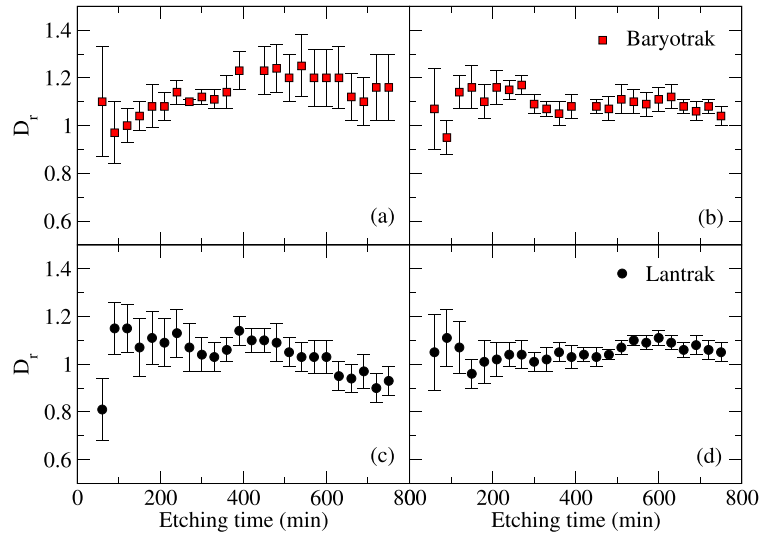
Fig. 1. Ratios of etch pit diameters (D_r) in detectors etched with NaOH + ethyl alcohol aqueous solution and NaOH (a) Baryotrak 80 °C, (b) Baryotrak 70 °C, (c) Lantrak 80 °C, and (d) Lantrak 70 °C.
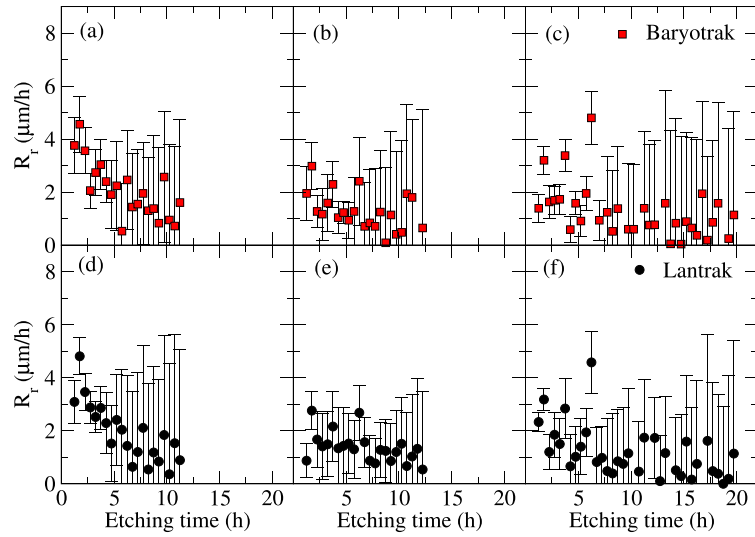

Fig. 2. Radial etch rates as function of the etching time for Baryotrak (red squares) and Lantrak (black dots) CR-39 detectors obtained at 80 °C for KOH ((a) and (d)), NaOH ((b) and (e)), and NaOH + ethyl alcohol ((c) and (f)) etching solutions.

The rate at which etch pit diameters grow is another quantity of interest. The radial etch rates (R_r) of alpha etch pits, defined as the etching rate perpendicular to the particle trajectory, evaluates the pit growth in the chemical etching process. It can be determined analyzing the variation of diameters from the radial growth of tracks with etching time through

$$R_r = \frac{D_{i+1} - D_i}{2\left(t_{i+1} - t_i\right)}, \tag{2}$$

where D_i and D_{i+1} are the alpha track diameters at t_i and t_{i+1} etching times, respectively. Figs. 2 and 3 show the radial etch rates of alpha tracks in Baryotrak and Lantrak CR-39 detectors at 80 °C and 70 °C, respectively.

For radial etch rates, obtained at 80 °C (see Fig. 2), the Baryotrak and Lantrak CR-39 detectors show similar patterns for each one of the etching solutions. However, the magnitudes and patterns of the radial etching rate plots slightly differ at different etching solutions, for the Baryotrak and Lantrak CR-39 detectors. Weak dips along the depth into both detectors are observed in radial etch rates for KOH and NaOH etching solutions, while such a trend is absent for the NaOH + ethyl

alcohol etching solution. Comparatively, the radial etch rates results for both Baryotrak and Lantrak CR-39 detectors are more systematic, intermediate and less systematic for the KOH, NaOH and NaOH + ethyl alcohol etching solution, respectively. Similar trends of radial etch rates with lower magnitudes are observed in Fig. 3, for the etching procedure at 70 °C, for both detectors and for all three etching solutions. The propagated uncertainties of the radial etch rates are quite large, as they involve the differences of relatively close mathematical quantities (e.g. etch pit diameters). In physical sense, there are two reasons for these large uncertainties: (i) radial growth being a slow process, which involves small variations over long etching time periods resulting in large uncertainties and (ii) energy variability of the moderated 1–2 MeV track forming alpha particles.

Figs. 4 and 5 show the ratios of diameters ($D_{L/B}$) and surface densities ($\rho_{L/B}$), respectively, of the Lantrak (L) to Baryotrak (B) alpha etch pits. Such ratios are defined through

$$D_{L/B} = \frac{D_L}{D_B}, \tag{3}$$
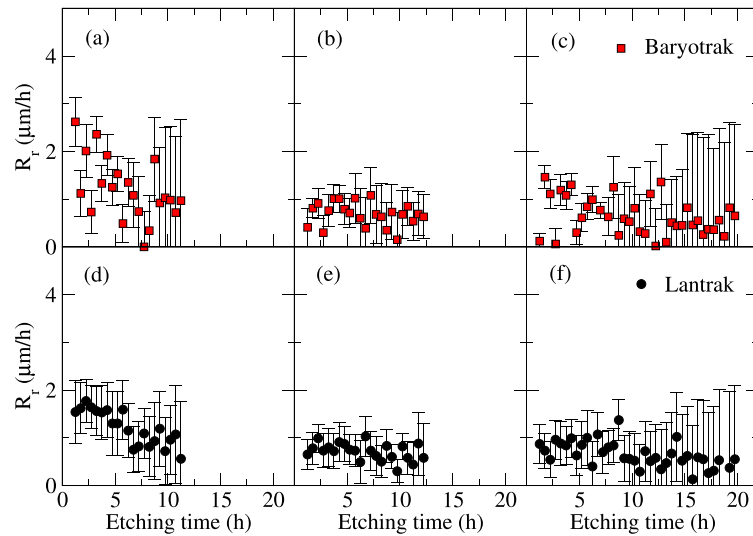
$$\rho_{L/B} = \frac{\rho_L}{\rho_B}, \tag{4}$$

Fig. 3. Radial etch rates (R_r) as function of the etching time for Baryotrak (red squares) and Lantrak (black dots) CR-39 detectors obtained at 70 °C for KOH ((a) and (d)), NaOH ((b) and (e)), and NaOH + ethyl alcohol ((c) and (f)) etching solutions.
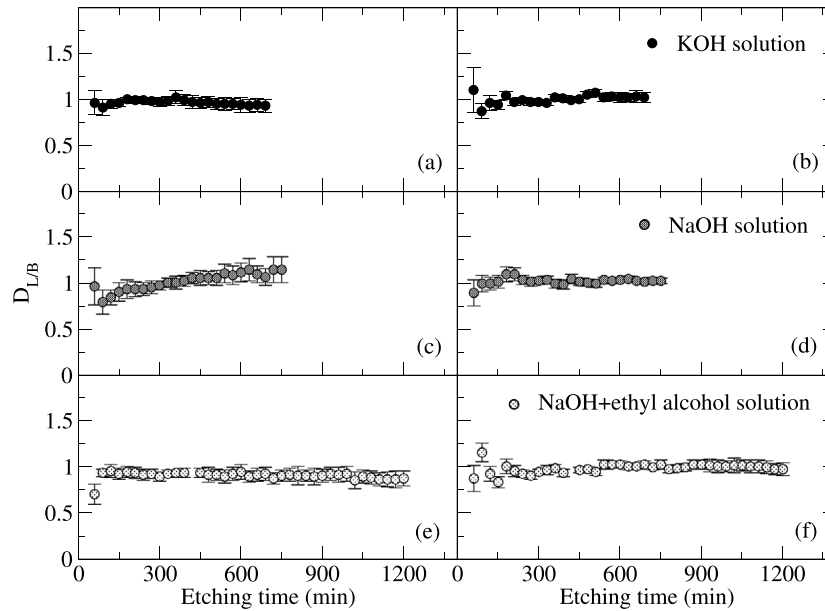

Fig. 4. Alpha track diameter ratio ($D_{L/B}$) as function of the etching time for the three aqueous solutions at (a), (c), (e) 80 °C and (b), (d), (f) 70 °C.

where D_L and D_B are the alpha track diameters, and ρ_L and ρ_B are the alpha track densities, with L and B standing for Lantrak and Baryotrak, respectively.

Fig. 4 clearly shows that the growth behavior of the alpha track is consistently the same for both types of CR-39 detectors under six different etching conditions. This is in agreement with the different results obtained by *Oliveira et al.* [31] and also shows the precision and reliability of the experimental results, not indicating any significant difference when we compare the track diameter of both detectors for each etching time.

Fig. 5 shows an increase of $\rho_{L/B}$, which is higher than unity, thereby indicating that the probability that the Lantrak receives alpha particles during the exposure was higher than that for to the Baryotrak. Due to the positioning of the Lantrak and Baryotrak detectors, their exposure geometries have been very similar, but not identical (see Figure 1 of the Ref. [31]). This could have influenced the observed difference.

Another relevant aspect about low-energy alpha particles is that in the range of 1 to 2 MeV there is a particular interest in investigations involving boron, as neutron converters in boron source/CR-39 sets [3,32,37], or boron doped CR-39 [38]. The energy of the alpha particles emitted in the ^{10}B(n, α)^{7}Li reaction is 1.47 MeV, which is in the middle of the energy range studied in this work. The choice of the best etching protocol will depend on the particularly intended application. In the examples already mentioned, the etch pit densities should be related with the neutron fluence [3] or absorbance [32] dose. In any case, etching/counting efficiency should be reproducible within a reasonably small range of temperatures. In this way, it is desirable that the diameter growth rate be as low as possible. If one expects the etch density to be high (approaching the detector saturation), the tracks should also be as smaller as possible. This condition is better fulfilled by the NaOH etching at 70 °C (Figs. 3-(b) and -(e)). On the other hand, if low etch pit densities are expected, then larger etch pit diameters are preferred. Among the tested conditions, the NaOH + ethyl alcohol
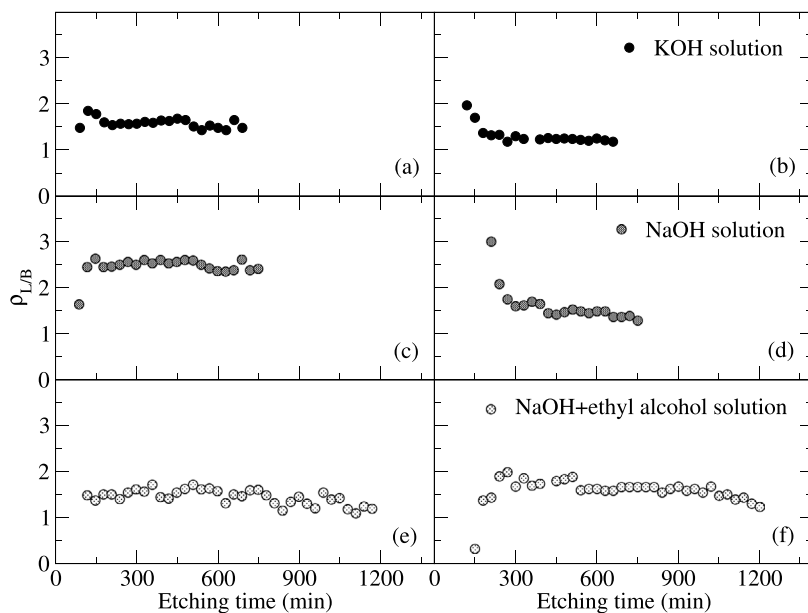
Fig. 5. Alpha track density ratio ($\rho_{L/B}$) as function of the etching time for the three aqueous solution at (a), (c), (e) 80 °C and (b), (d), (f) 70 °C.
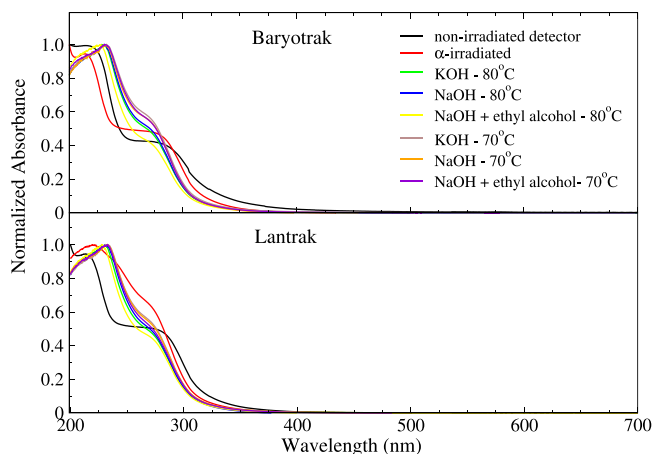

Fig. 6. Normalized absorbance spectra obtained from UV–Vis measurements for non-irradiated, α-irradiated and α-irradiated/etched detectors.

Table 1
Direct band-gap (E_g) values for Lantrak and Baryotrak detectors at different conditions.

Detector condition	E_g (eV)	
	Lantrak	Baryotrak
non-irradiated	3.98 ± 0.03	3.87 ± 0.04
α-irradiated	4.02 ± 0.03	3.98 ± 0.03
KOH - 70 °C	3.98 ± 0.03	4.02 ± 0.04
NaOH - 70 °C	4.06 ± 0.04	4.11 ± 0.05
NaOH+alcohol - 70 °C	4.07 ± 0.04	4.10 ± 0.04
KOH - 80 °C	4.04 ± 0.05	4.07 ± 0.05
NaOH - 80 °C	4.10 ± 0.05	4.11 ± 0.04
NaOH+alcohol - 80 °C	4.06 ± 0.05	4.12 ± 0.05

solution at 80 °C produces larger etch pits (Fig. 1), with smaller growth rates (Figs. 2-(c) and -(f)).

3.2. UV–Vis and Raman spectroscopy

The study of the UV–Visible and Raman spectra are valuable in verifying damage induced by irradiation of alpha particles in CR-39 detectors. Measurements have been carried out using the same Lantrak and Baryotrak CR-39 detectors corresponding to the last stage of the etching process presented by *Oliveira et al.* [31], performed using NaOH, KOH, and NaOH + ethyl alcohol chemical solutions at 70 ° and 80 °C. In addition, detectors with and without α-irradiation, not submitted to any previous chemical etching treatment, have also been employed in the measurements, called here non-irradiated and α-irradiated detectors. The normalized results obtained using the UV–Vis technique are shown in Fig. 6.

Fig. 6 shows the normalized absorbance spectra from the non-irradiated, α-irradiated and α-irradiated/etched Baryotrak (top) and Lantrak (bottom) detectors. Results show that both detectors present increased absorption on the short-wavelength side (lower than 400 nm)

being transparent in the visible energy range. The absorption bands in the range of 200–370 nm could be assigned to possible electronic transitions of $n \rightarrow \pi^*$ and $\pi \rightarrow \pi^*$, related to unsaturated centers of the molecules such as double bonds of C=C and C=O [39–41].

Table 1 shows the optical band-gap energy (E_g) values for each detector calculated by using the *Tauc* equation [42].

The band-gap has been evaluated considering direct allowed transitions. The direct band-gap energies for the Lantrak detectors are 3.98 ± 0.03 eV for the non-irradiated detector and 4.02 ± 0.03 eV for the α-irradiated one. Considering the uncertainties, the variation between the direct band-gap energy values of the α-irradiated and that of the non-irradiated detector does not show a significant difference, thereby indicating that there is no pronounced variation of the band-gap due to irradiation by low alpha particles fluency. In the case of the Baryotrak detectors, the calculated band-gap is 3.87 ± 0.04 eV for the non-irradiated, and 3.98 ± 0.03 eV for the α-irradiated detector. Results revealed that the non-irradiated Baryotrak detector has a lower band-gap value compared with the Lantrak one. In addition, results also show a small increase in the band-gap value for both α-irradiated/etched detectors. The optical results suggest that the Baryotrak and Lantrak CR-39 detectors have low sensitivity to the potential structural modifications resulting from the exposure to low fluency alpha particles irradiation and etching solutions at different temperatures in the fundamental absorption edge.

Raman spectra measurements have been carried out using the non-irradiated, α-irradiated and α-irradiated/etched CR-39 Lantrak and Baryotrak detectors in order to investigate structural modifications
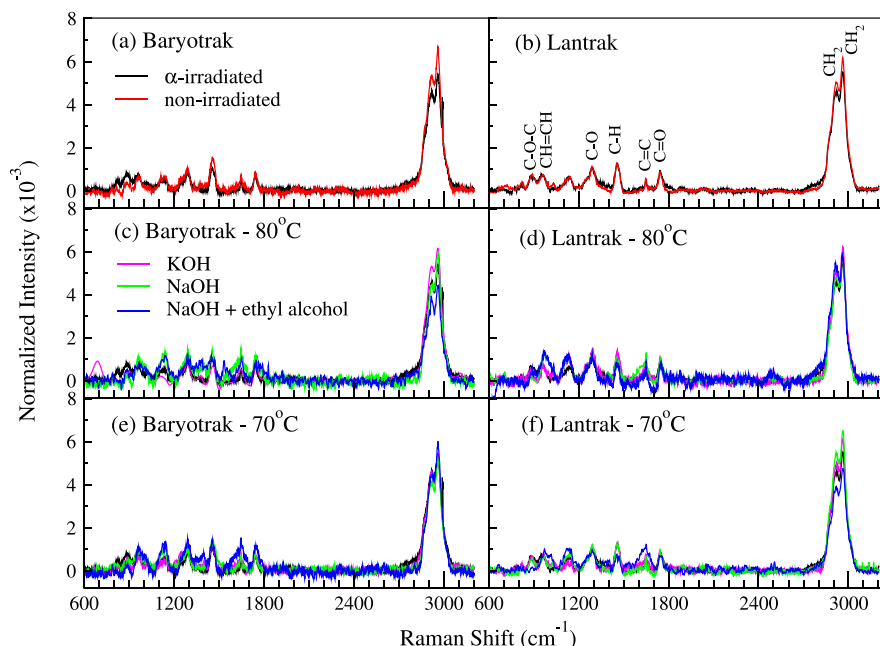
Fig. 7. Raman measurements for Lantrak and Baryotrak CR-39 detectors etched using KOH, NaOH and NaOH + ethyl alcohol at 80 °C and 70 °C compared with results obtained with non-irradiated and α-irradiated detectors.

induced by the irradiation and also by applied chemical treatments. The spectra from α-irradiated/etched detectors have been registered on the exposed side of α-irradiation and inside the tracks images. Results obtained with the Raman spectroscopy are illustrated on Fig. 7.

These spectra are used to evaluate the effects of the exposure to alpha radiation and etching solutions on the polymeric chain of the detectors. A strong contribution of fluorescence has been observed mainly for the etched detectors, which has been removed from the spectra applying the baseline correction. The observed prominent peaks are identified in Fig. 7-(b). More intense Raman modes corresponds to the anti-symmetric (2960 cm^{-1}) and symmetric (2920 cm^{-1}) vibrations assigned to the CH$_2$ group; the band located at 1741 cm^{-1} is assigned to the stretching vibration from the C=O group, to C=C at 1650 cm^{-1}. The band relative to the C–O group stands at 1292 cm^{-1}; in addition, the symmetrical stretching vibration around 889 cm^{-1} is associated to the C–O–C group. The band located at around 960 cm^{-1} corresponds to the CH=CH out of plane deformation. The band located around 1455 cm^{-1} is assigned to the C–H bending mode [43–51]. All the observed Raman bands attest the chemical structure of the CR-39 polymer on all detectors [52,53].

Furthermore, Fig. 7-(a,b) compares the Raman spectra from the non-irradiated and α-irradiated Baryotrak and Lantrak detectors. Results show variations in the CH$_2$ band and a slight increase in the C=C band for the irradiated Baryotrak detector compared to the non-irradiated one. As pointed out by *Yamauchi et al.* and *Pereira et al.*, the intensity of the CH$_2$ bands is directly correlated to the CH$_2$ group density and their intensity reduction reveals the loss of this group, suggesting the breaking of the polymer chain [43,44]. Fig. 7-(c–f) compares the Raman spectra from the α-irradiated and α-irradiated/etched detectors. Results show that the intensity of the CH$_2$ band is most affected in detectors submitted to NaOH + ethyl alcohol chemical etching at 80 °C for the Baryotrak detector. For the Lantrak, the decrease in the CH$_2$ band intensity has been more evident to detectors submitted to chemical etching at 70 °C. In both cases, the damage to the structure is more evident for detectors etched with NaOH + ethyl alcohol solution.

The obtained results from Lantrak and Baryotrak detectors reveal some change in the material structure induced by alpha particles irradiation, mainly for the Baryotrak detectors. In addition, results show that the CH$_2$ band intensity is affected by the chemical etching

solution and etching temperature. Based on this, an important point to be mentioned is the fact that the etching time has been different for each chemical solution, i.e., 700 min for the KOH solution, 750 min for the NaOH, and 1200 min for the NaOH + ethyl alcohol solution [31]. For the Baryotrak detectors etched at 80 °C, those submitted to the KOH chemical solution present a higher intensity for the CH$_2$ bands, indicating a lower degradation. On the other hand, the detector etched with NaOH + ethyl alcohol solution showed the greatest degradation. For the Baryotrak detectors, it is more perceptible that the damage is directly related to the etching time, where a higher etching time induces more damage in the polymer molecular structure. Based on the CH$_2$ band intensity, a significant damage is observed for the Lantrak detectors etched at 70 °C using the NaOH + ethyl alcohol solution. Negligible damage has been observed in the Lantrak detectors etched with the NaOH chemical solution at 70 °C.

The observed results suggest that the structural modifications can be potentially related to cross-linking and main chain scissions effects depends on the etching solution, temperature and etching time.

4. Conclusions

This work has provided a deeper look into the experimental data by *Oliveira et al.* [31], based on chemical etching studies using CR-39 track detectors bombarded with low energy alpha particles. Valuable new analysis and worthy new results have been obtained. In addition, new measurements and analysis with UV–Visible and Raman spectroscopy shed light on the possible mechanisms underlying the efficiency variations.

The response of the CR-39 detectors to 1–2 MeV energy alpha particles has been characterized by in-depth quantitative analysis of the alpha etch pit diameter ratio (D$_r$) and radial etch rates (R$_r$) for three different chemical etching solutions at two temperatures. The ratio plots of both alpha track diameters ($D_{L/B}$) and surface alpha track densities ($\rho_{L/B}$) were proved to be important in verifying the consistency of the results obtained for the analyzed conditions. An invariable behavior for the six different analyzed chemical etching conditions (three solutions at two different temperatures) has been observed. These results are in full agreement with the conclusions by *Oliveira et al.* [31], evidencing the accuracy and trustworthiness of the experimental data. This is a

remarkable fact, since measurements with NDT detectors are known to be difficult to reproduce, due to the environmental parameters (temperature control, solution evaporation during development, and even the uniform exposure of detectors). In the analysis of the density ratio ($\rho_{L/B}$), some variations have been observed, probably due to the fact that the Lantrak and Baryotrak CR-39 detectors have not been exposed to exactly the same geometry (see Figure 1 of Ref. [31]). Moreover, the effect of the addition of the ethyl alcohol to the NaOH etching solution potentiates the chemical etching, thereby accelerating the growth of etch pit diameters, here evaluated from the radial alpha track growth, D_r. Therefore, the Baryotrak detector is more sensitive to the addition of the alcohol to the solution, but it has a lower detection efficiency, as compared to the Lantrak one.

In addition to the exploratory analysis of the data by *Oliveira et al.* [31], we have proceeded to the new UV–Vis and a Raman spectroscopy measurements for the non-irradiated, α-irradiated and α-irradiated/etched Lantrak and Baryotrak detectors (KOH, NaOH and NaOH + ethyl alcohol solutions at 70 and 80 °C). The direct band-gap energies have been determined for all Lantrak and Baryotrak detectors showing only small modifications for detectors subjected to different etching conditions. In addition, the Raman obtained results reveal that the CH_2 band intensity depends on the etching time, as observed by *Pereira et al.* [43], and the effect of the etching temperature depends on the detector type. Additionally, in some cases a small increase in the C=C band has been noted. The observed modifications suggest that cross-linking and main chain scissions affects the Lantrak and Baryotrak structure.

The good detection efficiency of the Lantrak detector, as obtained by using different solutions and temperatures, as already mentioned by *Oliveira et al.* [31], has been confirmed in the quantitative analysis performed in our work. These measurements have been essential to elucidate the problem of the intrinsic detection efficiency of both Lantrak and Baryotrak CR-39 detectors, as noted by Ref. [31]. Furthermore, it may even serve as a protocol for use of these track detectors in their known applications. In perspective, our results could be useful to the detection of low energy neutrons through the neutron-alpha ^{10}B(n, α)^{7}Li reaction, which is significant in nuclear safety.

Declaration of competing interest

The authors declare that they have no known competing financial interests or personal relationships that could have appeared to influence the work reported in this paper.

Acknowledgments

References

[1] S.A. Durrani, R.K. Bull, Solid State Nuclear Track Detection: Principles, Methods, and Applications, Pergramon Press, 1987, URL http://refhub.elsevier.com/S0168-9002(21)00114-5/sb21.

[2] C. Baccou, V. Yahia, S. Depierreux, C. Neuville, C. Goyon, F. Consoli, R. De Angelis, J.E. Ducret, G. Boutoux, J. Rafelski, C. Labaune, CR-39 track detector calibration for H, He, and C ions from 0.1-0.5 MeV up to 5 MeV for laser-induced nuclear fusion product identification, Rev. Sci. Instrum. 86 (2015) 083307, http://dx.doi.org/10.1063/1.4927684.

[3] B. Smilgys, S. Guedes, M. Morales, F. Alvarez, J.C. Hadler, P.R.P. Coelho, P.T.D. Siqueira, I. Alencar, C.J. Soares, E.A.C. Curvo, Boron thin films and CR-39 detectors in BNCT: A method to measure the ^{10}B(n, α)^{7}Li reaction rate, Radiat. Meas. 50 (2013) 181–186, http://dx.doi.org/10.1016/j.radmeas.2012.07.001.

[4] H.A. Khan, T. Lund, P. Vater, R. Brandt, J.W.N. Tuyn, Some gross features of the interaction of semirelativistic ^{16}O and ^{12}C ions with ^{197}Au targets, Phys. Rev. C 28 (4) (1983) 1630–1634, http://dx.doi.org/10.1103/PhysRevC.28.1630.

[5] S. Guedes, J.C. Hadler, P.J. Iunes, S.R. Paulo, C.A.S. Tello, On the reproducibility of SSNTD track counting efficiency, Nucl. Instrum. Methods Phys. Res. B 418 (2) (1998) 429–433, http://dx.doi.org/10.1016/S0168-9002(98)00918-8.

[6] M.A. Rana, How to achieve precision and reliability in experiments using nuclear track detection technique? Nucl. Instrum. Methods Phys. Res. A 592 (3) (2008) 354–360, http://dx.doi.org/10.1016/j.nima.2008.04.025.

[7] T. Yamauchi, Studies on the nuclear tracks in CR-39 plastics, Radiat. Meas. 36 (1–6) (2003) 73–81, http://dx.doi.org/10.1016/S1350-4487(03)00099-4.

[8] R. Kwiatkowski, A. Malinowska, M. Gierlik, J. Rzadkiewicz, A. Szydlowski, A. Urban, K. Mikszuta, Assessment of 14 MeV DT neutron generator emission with activation and particle track methods, Fusion Eng. Des. 146 (2019) 1060–1063, http://dx.doi.org/10.1016/j.fusengdes.2019.02.002.

[9] M.A. Rana, CR-39 nuclear track detector: An experimental guide, Nucl. Instrum. Methods Phys. Res. A 910 (2018) 121–126, http://dx.doi.org/10.1016/j.nima.2018.08.077.

[10] F. Assenmacher, M. Boschung, E. Hohmann, S. Mayer, Comparison of different PADC materials and etching conditions for fast neutron dosimetry, Radiat. Prot. Dos. 170 (1–4) (2016) 162–167, http://dx.doi.org/10.1093/rpd/ncv421.

[11] D. Hermsdorf, Physics aspects of light particle registration in PADC detectors of type CR-39, Rad. Meas. 46 (4) (2011) 396–404, http://dx.doi.org/10.1016/j.radmeas.2011.02.012.

[12] K.F. Chan, F.M.F. Ng, D. Nikezic, K.N. Yu, Bulk and track etch properties of CR-39 SSNTD etched in NaOH/ethanol, Nucl. Instrum. Methods Phys. Res. B 263 (1) (2007) 284–289, http://dx.doi.org/10.1016/j.nimb.2007.04.148.

[13] J.C. Hadler, S.R. Paulo, Indoor radon daughter contamination monitoring - The absolute efficiency of CR-39 taking into account the plateout effect and environmental-conditions, Radiat. Prot. Dosim. 51 (4) (1994) 283–296, http://dx.doi.org/10.1093/oxfordjournals.rpd.a082146.

[14] M.A. Rana, CR-39 nuclear track detector: An experimental guide, Nucl. Instrum. Methods Phys. Res. A 910 (2018) 121–126, http://dx.doi.org/10.1016/j.nima.2018.08.077.

[15] B.G. Cartwright, E.K. Shirk, P.B. Price, A nuclear-track-recording polymer of unique sensitivity and resolution, Nucl. Instrum. Methods 153 (2) (1978) 457–460, http://dx.doi.org/10.1016/0029-554X(78)90989-8.

[16] G. Espinosa, L. Font, M. Fromm, A review of the developments in nuclear track methodology as published in the proceedings of the international conference on nuclear tracks in solids from 1990 to 2008, in: 25th Int. Conf. on Nuclear Tracks in Solids, Vol. 50, Elsevier, Puebla, Mexico, 2011, pp. 1–6, URL https://hal.archives-ouvertes.fr/hal-00821904.

[17] R. Félix-Bautista, C. Hernández-Hernández, B.E. Zendejas-Leal, R. Fragoso, J.I. Golzarri, C. Vázquez-López, G. Espinosa, Evolution of etched nuclear track profiles of alpha particles in CR-39 by atomic force microscopy, Radiat. Meas. 50 (2013) 197–200, http://dx.doi.org/10.1016/j.radmeas.2013.01.002.

[18] I.S. Simakin, I.E. Vlasova, S.N. Kalmykov, Digital image analysis of the etched α-tracks in CR-39, Radiat. Meas. 50 (2013) 212–217, http://dx.doi.org/10.1016/j.radmeas.2012.11.013.

[19] G. Immè, D. Morelli, M. Aranzulla, R. Catalano, G. Mangano, Nuclear track detector characterization for alpha-particle spectroscopy, Radiat. Meas. 50 (2013) 253–257, http://dx.doi.org/10.1016/j.radmeas.2012.03.014.

[20] A. Szydlowski, A. Malinowska, M. Jaskola, A. Korman, K. Malinowski, M. Kuk, Calibration studies and the application of nuclear track detectors to the detection of charged particles, Radiat. Meas. 50 (2013) 258–260, http://dx.doi.org/10.1016/j.radmeas.2012.03.013.

[21] A.P. Fews, D.L. Henshaw, High resolution alpha particle spectroscopy using CR-39 plastic track detector, Nucl. Instrum. Methods Phys. Res. 197 (2–3) (1982) 517–529, http://dx.doi.org/10.1016/0167-5087(82)90349-0.

[22] M. Sohrabi, G. Zainali, Broadening registration energy range of alpha tracks in CR-39 under a new ECE condition, Int. J. Radiat. Appl. Instrum. Part D. Nucl. Tracks Radiat. Meas. 12 (1) (1986) 171–174, http://dx.doi.org/10.1016/1359-0189(86)90564-9.

[23] S. Bing, CR-39 radon detector, Nucl. Tracks Radiat. Meas. 22 (1–4) (1993) 451–454, http://dx.doi.org/10.1016/0969-8078(93)90106-E.

[24] O.A.P. Tavares, M.L. Terranova, Alpha activity of ^{190}Pt isotope measured with CR-39 track detector, Radiat. Meas. 27 (1) (1997) 19–25, http://dx.doi.org/10.1016/S1350-4487(96)00154-0.

[25] B. Dörschel, D. Hermsdorf, U. Reichelt, S. Starke, Y. Wang, 3D computation of the shape of etched tracks in CR-39 for oblique particle incidence and comparison with experimental results, Radiat. Meas. 37 (6) (2003) 563–571, http://dx.doi.org/10.1016/S1350-4487(03)00243-9.

[26] D. Nikezic, K.N. Yu, Calculations of track parameters and plots of track openings and wall profiles in CR39 detector, Radiat. Meas. 37 (6) (2003) 595–601, http://dx.doi.org/10.1016/S1350-4487(03)00080-5.

[27] M.A. Rana, On problems in trustworthy predictions of etched track parameters, Radiat. Meas. 43 (9–10) (2008) 1546–1549, http://dx.doi.org/10.1016/j.radmeas.2008.09.002.

[28] A.A. Azooz, S.H. Al-Nia'emi, M.A. Al-Jubbori, A parameterization of nuclear track profiles in CR-39 detector, Comput. Phys. Comm. 183 (11) (2012) 2470–2479, http://dx.doi.org/10.1016/j.cpc.2012.06.011.

[29] D.H. Fan, W.H. Zhuo, B. Chen, W.Y. Zhang, Uncertainty of an automatic system for counting alpha tracks on CR-39, Nucl. Sci. Techn. 28 (11) (2017) 1–6, http://dx.doi.org/10.1007/s41365-017-0314-8.

[30] S.S. Chavan, A.M. Mhatre, A.K. Pandey, H.K. Bagla, Alpha track registration and revelation in CR-39 using new etching method for ultratrace alpha radioactivity quantification in solution media, Radiochim. Acta 109 (6) (2021) 503–512, http://dx.doi.org/10.1515/ract-2020-0010.

[31] C.S. Oliveira, B. Malheiros, K.C.C. Pires, M. Assunçao, S. Guedes, J.N. Corrêa, S.A. Paschuk, Low energy alpha particle tracks in CR-39 nuclear track detectors: Chemical etching studies, Nucl. Instrum. Methods Phys. Res. A 995 (2021) 165130, http://dx.doi.org/10.1016/j.nima.2021.165130.

[32] I. Traoré, A. Nachab, A. Nourreddine, A. Bâ, Characterization of a PN3 personal neutron dosimeter based on (n,α) reaction, Results Phys. 5 (2015) 144–147, http://dx.doi.org/10.1016/j.rinp.2015.05.002.

[33] M.T. Barrera, H. Barros, F. Pino, J. Davila, L. Sajo-Bohus, Thermal and epithermal neutron fluence rate gradient measurements by PADC detectors in linac radiotherapy treatments-field, in: 11th International Symposium on Radiation Physics (ISRP), in: AIP Conference Proceedings, vol. 1671, 2015, http://dx.doi.org/10.1063/1.4927191.

[34] H. Tanaka, Y. Sakurai, M. Suzuki, S. Masunaga, K. Takamiya, A. Maruhashi, K. Ono, Development of a simple and rapid method of precisely identifying the position of B-10 atoms in tissue: An improvement in standard alpha autoradiography, J. Radiat. Res. 55 (2) (2014) 373–380, http://dx.doi.org/10.1093/jrr/rrt110.

[35] X. Wang, J.D. Brockman, J.M. Guthrie, S.Z. Lever, Analysis and imaging of boron distribution in maize by quantitative neutron capture radiography, Appl. Radiat. Isot. 140 (2018) 252–261, http://dx.doi.org/10.1016/j.apradiso.2018.07.028.

[36] C.J. Soares, I. Alencar, S. Guedes, R.H. Takizawa, B. Smilgys, J.C. Nadler, Alpha spectrometry study on LR115 and Makrofol through measurements of track diameter, Radiat. Meas. 50 (2013) 246–248, http://dx.doi.org/10.1016/j.radmeas.2012.06.010.

[37] A.P. Bonifaz, O.B. Molin, J.O. Schneider, B.L. La Rosa, J.R. Hancco, V.G. Rojas, D.P. Fernandez, P.P. Anaya, M.E.L. Herrera, Simple and low cost alternative method for detecting photoneutrons produced in some radiotherapy treatments using SSNTDs, Appl. Radiat. Isot. 161 (2020) http://dx.doi.org/10.1016/j.apradiso.2020.109169.

[38] V.M. Pawar, M. Bcek, A.D. Shetgaonkar, R. Pal, A.K. Bakshi, V.S. Nadkarni, Synthesis and application of boron polymers for enhanced thermal neutron dosimetry, Nucl. Instrum. Methods Phys. Res. Sec. B-Beam Interactions Mater. Atoms 462 (2020) 169–176, http://dx.doi.org/10.1016/j.nimb.2019.11.011.

[39] M.E. Ghazaly, H. Hassan, Spectroscopic studies on alpha particle-irradiated PADC (CR-39 detector), Results Phys. 4 (2014) 40–43, http://dx.doi.org/10.1016/j.rinp.2014.04.001.

[40] D.L. Pavia, G.M. Lampman, G.S. Kriz, Introduction to Spectroscopy, second ed., Harcourt Brace College Publishers, 1994.

[41] A.M. Abdalla, F.A. Harraz, S. Al-Sayari, A. Al-Hajry, Structural and optical investigation on alpha particle irradiated CR-39 surface coated by MEH-PPV conducting polymer, Appl. Surf. Sci. 347 (2015) 685–689, http://dx.doi.org/10.1016/j.apsusc.2015.04.003.

[42] D.L. Wood, J. Tauc, Weak absorption tails in amorphous semiconductors, Phys. Rev. B 5 (1972) 3144–3151, http://dx.doi.org/10.1103/PhysRevB.5.3144.

[43] L.A.S. Pereira, C.A.T. Sáenz, C.J.L. Constantino, E.A.C. Curvo, A.N.C. Dias, C.J. Soares, S. Guedes, Micro-Raman spectroscopic characterization of a CR-39 detector, Appl. Spectrosc. 67 (4) (2013) 404–408, http://dx.doi.org/10.1366/12-06741.

[44] T. Yamauchi, S. Takada, H. Ichijo, K. Oda, Raman and near-IR study on proton irradiated CR-39 detector and the effect of air-leak on damage formation, Radiat. Meas. 34 (1) (2001) 69–73, http://dx.doi.org/10.1016/S1350-4487(01)00123-8.

[45] Z. Zhu, Y. Sun, C. Liu, J. Liu, Y. Jin, Chemical modifications of polymer films induced by high energy heavy ions, Nucl. Instrum. Methods Phys. Res. B 193 (1) (2002) 271–277, http://dx.doi.org/10.1016/S0168-583X(02)00773-5.

[46] L.J. Bellamy, The Infrared Spectra of Complex Molecules, vol. 1, John Wiley and Sons, New York, 1975.

[47] G. Socrates, Infrared Characteristic Group Frequencies, John Wiley and Sons, New York, 1980.

[48] T. Phukan, D. Kanjilal, T.D. Goswami, H.L. Das, Study of optical properties of swift heavy ion irradiated PADC polymer, Radiat. Meas. 36 (1) (2003) 611–614, http://dx.doi.org/10.1016/S1350-4487(03)00210-5.

[49] N.L. Singh, A. Qureshi, F. Singh, D.K. Avasthi, Modifications of polycarbonate induced by swift heavy ions, Mater. Sci. Eng. A 457 (1) (2007) 195–198, http://dx.doi.org/10.1016/j.msea.2006.12.008.

[50] K.C.C. Tse, F.M.F. Ng, D. Nikezic, K.N. Yu, Bulk etch characteristics of colorless LR 115 SSNTD, Nucl. Instrum. Methods Phys. Res. B 263 (1) (2007) 294–299, http://dx.doi.org/10.1016/j.nimb.2007.04.308.

[51] J.W. Mitchell, A. Addagada, Chemistry of proton track registration in cellulose nitrate polymers, Radiat. Phys. Chem. 76 (4) (2007) 691–698, http://dx.doi.org/10.1016/j.radphyschem.2006.05.012.

[52] R. Sagheer, M.S. Rafique, F. Saleemi, S. Arif, F. Naab, O. Toader, A. Mahmood, R. Rashid, I. Hussain, Modification in surface properties of poly-allyl-diglycol-carbonate (CR-39) implanted by Au ions at different fluences, Mater. Sci.-Poland 34 (2) (2016) 468–478, http://dx.doi.org/10.1515/msp-2016-0067.

[53] V. Kumar, P.K. Goyal, S. Mahendia, R. Gupta, T. Sharma, S. Kumar, Tuning of the refractive index and optical band gap of CR-39 polymers by heating, Radiat. Eff. Defects Solids 166 (2) (2011) 109–113, http://dx.doi.org/10.1080/10420151003587385.